Copyright Warning & Restrictions

The copyright law of the United States (Title 17, United States Code) governs the making of photocopies or other reproductions of copyrighted material.

Under certain conditions specified in the law, libraries and archives are authorized to furnish a photocopy or other reproduction. One of these specified conditions is that the photocopy or reproduction is not to be "used for any purpose other than private study, scholarship, or research." If a, user makes a request for, or later uses, a photocopy or reproduction for purposes in excess of "fair use" that user may be liable for copyright infringement,

This institution reserves the right to refuse to accept a copying order if, in its judgment, fulfillment of the order would involve violation of copyright law.

Please Note: The author retains the copyright while the New Jersey Institute of Technology reserves the right to distribute this thesis or dissertation

Printing note: If you do not wish to print this page, then select "Pages from: first page # to: last page #" on the print dialog screen

ABSTRACT

FLEXIBLE MICROFLUIDIC DEVICE WITH NONPLANAR INTERDIGITATED MICROELECTRODES

The lab-on-a-chip concept has improved significantly in recent years to meet global demand for various applications with the advent of new technologies. Much progress has been achieved, but many microfluidic devices still suffer from design limitations in terms of sensitivity and selectivity because they use rigid, fragile substrate materials and conventional electrodes, which do not provide high sensitivity or selectivity and suffer from signal-to-noise ratio issues. This work proposes a novel device architecture that uses flexible, transparent top and bottom layers integrated with (nonplanar interdigitated microelectrodes) to create a sandwich-like flexible substrate base. The top and bottom layers consist of 3D nonplanar interdigitated microelectrodes developed using soft lithography and deposited over transparent flexible materials such as polydimethylsiloxane, polyethylene terephthalate, or polybutylene adipate terephthalate (e.g., eco flex) Polyethylene terephthalate (PET). We created the middle layer composed of microfluidic channels using flexible polypropylene double-sided adhesive layer tape. This device's design, which involves nonplanar interdigitated microelectrodes over transparent flexible and stretchable material and flexible microfluidic channels, provides the following advantages over conventional devices: (a) a flexible design involving flexible materials that make it wearable and could be used in embedded systems and (b) high sensitivity resulting from nonplanar microelectrodes with different configurations that improve the electric field in the microfluidic channels. Furthermore, we can use various materials in the microfluidic channels, such as metal-organic-framework (MOF), as transducers to improve the signal-to-noise ratio, sensitivity, and selectivity. We also show that optical and electrochemical methods such as CV, EIS, and DPV could create a multipurpose device and embedded system. Finally, we show the device's sensitivity and selectivity limits.

FLEXIBLE MICROFLUIDIC DEVICE WITH NONPLANAR INTERDIGITATED MICROELECTRODES

by
Saud Alssaidy

A Dissertation
Submitted to the Faculty of
New Jersey Institute of Technology
in Partial Fulfillment of the Requirements for the Degree of
Master of Science in Materials science and engineering

Otto H. York Department of Chemical and Materials Engineering

December 2021

APPROVAL PAGE

FLEXIBLE MICROFLUIDIC DEVICE WITH NONPLANAR INTERDIGITATED MICROELECTRODES

Saud Alssaidy

Dr. Sagnik Basuray, Thesis Advisor — Date
Associate Professor Chemical & Materials Engineering, NJIT

Dr. Roman S. Voronov, Thesis Committee Member — Date
Associate Professor of Chemical & Materials Engineering, NJIT

Dr. Piero M. Armenante, Thesis Committee Member — Date
Distinguished Professor, Chemical & Materials Engineering, NJIT

BIOGRAPHICAL SKETCH

Author: Saud Alssaidy

Degree: Master of Science

Date: December 2021

Undergraduate and Graduate Education:

- Master of Science in Materials Science and Engineering.
  New Jersey Institute of Technology, Newark, NJ, 2021

- Bachelors in Chemicals and Materials Engineering.
  King Abdul Aziz University, Jeddah, 2016

Major: Materials Science and Engineering

Presentation and conferences:

- NFS-ICORPS NJIT Site Program: Business Thesis: A Point-of-Care (POC) Device Providing Real-Time Results to Potential COVID-19 Patients.
- International Conference on Advanced Materials and Their Application: Flexible Microfluidic Device With Nonplanar Interdigitated Microelectrodes.

I dedicate this thesis to almighty God, my beloved parents, my family, and all who supported me in my journey.

ACKNOWLEDGMENT

I want to thank Prof. Sagnik Basuray, my thesis advisor, for his continuous support. I have learned much from his suggestions and inspiration ideas; moreover, he answered all my questions and concerns and made my thesis journey more enjoyable.

Thank committee members Dr. Roman S. Voronov and Dr. Piero M. Armenante for their time, and I sincerely appreciate their support and valuable time.

Thank Dr. Charmi Chande for her support and valuable time, suggestions, and guidance in my thesis work.

I want to thank the Saudi Arabian Cultural Mission (SACM), King Abdul-Aziz University, for their support, specifically Prof. Ali Morfeq, Prof. Ahmed Alssaidi, and Prof. Fouad Alssaidi, Dr. Mustafa Zyadi, and the university president Prof. Abdulrahman Al-Youbi.

I want to thank the Advanced Science Research Center at the Graduate Center of the City University of New York for giving me a chance to use their facilities.

I want to thank Li Zhenglong, Cheng, Yu Hsuan, and all my friends who have supported me throughout my master's.

TABLE OF CONTENTS

LIST OF TABLES

Table **Page**

LIST OF FIGURES

CHAPTER 1

INTRODUCTION

1.1 Background Information

Lab on chip (LOC) device includes a micrometer device or smaller device to extrapolate single or multiple laboratory experiments on the same platform. It mainly involves the concept of microfluidics which deals with the study of behavior, control, and manipulation of fluids at the scale of sub-millimeter to micrometer range. LOC devices have been widely exploited in molecular diagnosis, biodefense, chemical analysis, and microelectronics. A microfluidics system's advantages are low sample and reagent volume, less reaction time, less energy consumption, high throughput analysis, low fabrication cost, and many more. These advantages make it easier to incorporate multiple experiments on the same LOC device. Also, controlled manipulation of fluid is possible by using instruments like syringe pumps or valve controllers. Furthermore, the entire investigation can be semi-automated or automated by using dedicated software to control the moment of fluids in a device like MATLAB or LabView. So, microfluidics can be successfully used for high throughput analysis.

A wide range of materials has been used to fabricate microfluidic devices. Glass and silicon were the first materials to manufacture the devices due to their availability and advanced micromachining processes. However, these materials were relatively expensive to process, brittle, and not self-sealing. The drawbacks associated with silicon and Glass led to the emergence of new flexible materials to deform, bend, and stretch under mechanical loads for manufacturing the next generation of microfluidic devices. Microchannels, microvalves, micropumps, micromixers, and many other components have employed flexibility due to advantages like versatile use of the device on different substates, ease to handle, and mass production with manufacturing process.

Microfluidic devices have made significant improvements in design, sensing materials, fabrication, performance, the use of different sensation materials, receptors, selectivity, the limit of detection, resolution, and the use of integrated sensors. All of which will be part of the next-generation technologies of the 21st century, such as space exploration, AI applications, and the Internet of Things. Cost, sensitivity, selectivity, size, and diagnosis speed are essential parameters to evaluate sensors. Currently, the health sector needs rapid, accurate, and sensitive detection techniques to speed up diagnostics. In addition, many viruses, such as those that cause Ebola, HIV, influenza, plague, and many other diseases, affect global health. Microfluidic devices are considered an essential defense against chemicals, pathogens, cancer, and many other things, such as the recent COVID-19 pandemic. Finally, Microfluidic devices have proven their ability to reduce the gap for sensitive economic equipment, making it affordable to increase health care efficiency worldwide to increase life quality and the ability to diagnose and control diseases in the early stages. Moreover, it provides rapid detection of environmental contamination. (Andryukov et al., 2020; Cheng et al., 2019; Duvvuri & Lood, 2019; Thompson et al., 2016; Chen et al., 2020).

1.2 Microfluidic Devices

Microfluidics could be defined as the designing and studying the physical and chemical properties of microchannels. A tiny amount of fluid goes through these microchannels. Different applications of microfluidics include sensors, instrumental analysis, advanced separation process, space applications, medical applications such as LOC and organs on the chips with high efficiency, fast result, friendly use, and low cost.

1.2.1 Sensors in Microfluidic Devices

In general, sensors consist of three essential components, viz. a receptor for accepting samples, a recognition molecule for testing the detected model, and a transducing material to convert the reaction into a quantitative response. Targets include but are not limited to enzymes, antibodies, nucleic acids, and DNA strands. Media could be either gas or liquid. Receptors and sensor materials consist of bioreceptors such as aptamers or non-bioreceptors such as carbon nanotube materials (CNTs). Signals systems convert the results of the reactions between target and sensor materials to signals. Finally, processors and interfaces programs convert signals and display results.

Biosensors are classified based on the recognition biomolecules such as antibodies, nucleic acids, antigens, and aptamers, immobilized on the sensor surface and create signals (Liu et al., 2018). The new generation of composite materials and polymers improve the design and reduce the cost of microfluidic devices, give the ability to modify the channels dimension, and the 3D printing approach can be applied with low operation cost than other materials. Conductive polymers and thin metal film on a flexible substrate are promised materials used in flexible sensors. (Seekaew et al., 2014; Tai et al., 2020).

1.2.2 Transducer Materials in Microfluidic Devices

Transducer materials are an essential part of a sensor's components. These materials control most of the sensor's features, starting with sensitivity, selectivity, response time, stability for the targeted application, and power saving. In addition, they convert the measurement into signals such as current, resistance, frequency, and voltage. There are many types of sensing materials, such as Metal Oxide Gas Sensing Material (MOS) with p or n types, which could be manufactured by a different process such as physical

vapor deposition (PVD) or chemical vapor deposition (CVD). In addition, MOS sensors could enhance power savings by using catalysts. CNTs are among the most excellent transducer materials for many reasons, such as sensitivity, selectivity, and their ability to work at room temperature. Further, the power requirement for CNT sensors is low. (Nazemi et al., 2019). Using sensor transducer materials such as CNTs, graphene, QDs, MOS, and MXenes materials can present more advantages among other materials like operation conditions and sensitivity (Hunter et al., 2020).

Interestingly most of the transducer materials use gold electrodes. Gold is an excellent electrode material due to its numerous benefits, such as stability, favorable electron transfer kinetics as a catalyst, convenient ability to form covalent bonds with functional groups such as thiols, and unique optical properties. This has been widely applied in sensor electrode materials due to their high stability.

1.3 Electrochemical based Microfluidic Sensors

Electrochemical sensors using microfluidics have expanded analytical chemists' ability to detect cells, proteins, DNA, small molecules, metal ions, and gas molecules. Electrochemical sensors usually contain a reference electrode, a working electrode, and a counter electrode. The reactions occur between the analyte and electrode, producing a measurable signal. Many electrochemical detection methods include cyclic voltammetry, differential pulse voltammetry, electrochemical impedance spectroscopy (EIS), fast-scan cyclic voltammetry, and square wave voltammetry (Khorramizadeh et al., 2019). Each technique has offered some advantages, either in sensitivity or selectivity. Electrochemical sensors have many benefits, such as low cost, high sensitivity, and ease of miniaturization. Recently advances in electrochemical methods in microfluidic devices have been made using several well-established fabrication techniques to produce ultrasensitive sensors (Cheng et al., 2019). This, combined with

the rapid response, cost-effectiveness, and real-time monitoring of the samples, electrochemical sensors have shown great promise as an ultrasensitive method for detecting low concentrations. However, the successful application of these sensors remains restricted to laboratory settings.

Recently there has been the development of photochemical sensors that combine electrochemistry with light to make more sensitive and selective sensors. The reactant determinant, electron transfer, and energy transfer are three essential principles that give researchers comprehensive design guidance to develop advanced photochemical biosensing sensors (Shu & Tang, 2020; Zang et al., 2017). A Photoelectrochemical imaging system can be used to investigate cell processes, examine the development of drug responses in tissue, engineer materials, and diagnose diseased cells (Wu et al., 2019). Selectivity, sensitivity, and time response are critical factors in the design and evaluation of these sensors.

1.4 Channel Geometry

Channel geometry is a critical parameter of how sensor components and target analytes are organized, react, and communicate together. Passive mixing, controlling fluids flow through the microchannels, and fluid pressure drop inside channels affect the selectivity

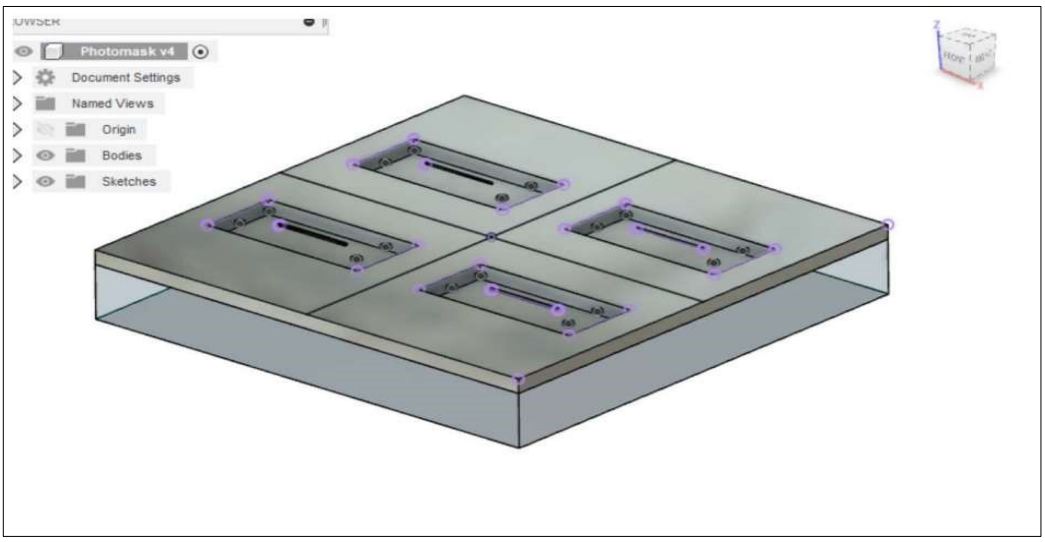

Figure 1.1. Photomask design by fusion 360 software.

and sensitivity of the sensor devices. In addition, many channels' geometries are used in sensors, such as curved spiral, staggered herringbone, and hybrid systems, which depend on the secondary flow and force inertia in microfluidics systems (Dhiraj et al., 2018). As a result, channels, geometry, and aspect ratio can enhance the shear force, increase the device efficiency, and remove fouling. Finally, there are different methods for making channels with specific dimensions and shapes, like using a photomask in Figure 1.

1.5 Microfluidic based Optical Sensors

Optical fiber sensors have different components depending on their applications. They contain various film-coated sensing nanocomposite materials such as MOS nanoparticles, piezoelectric materials, graphene oxides, and CNTs. In addition, optical sensors, including visual and photonic fiber-crystal gas sensors, detect light propagation through the device (Nazemi et al., 2019; Pawar & Kale, 2019). However, despite these advantages, optical fiber sensors have limitations in terms of miniaturization due to the size of optical fibers. Fortunately, transparent flexible materials substrate could enhance and improve its functionality.

Optical sensor measurement signals depend on the reaction between the electromagnetic spectrum and materials (e.g., transmission, reflection, and scattering). The sensitivity of optical sensors depends on changes in light, such as absorbance or intensity. They combine microfluid chips and optical systems such as high-power ultraviolet LED. The light field formed enhances the interaction between light and fluid (Chin et al., 2008; Lapsley et al., 2011; Yoon & Kim, 2012). Electrical detection consists of several conductivity, dynamic, and impedance techniques. Optical detection mainly consists of fluorescence, absorption, and Infrared Spectroscopy (IR) detection. The optic sensor

showed a high sensitivity for samples of DNA with very tiny concentrations in the microfluidic device. It has high selectivity, sensitivity, and stability. It has many applications, such as detecting Volatile organic compounds (VOCs), biomolecules, and microfluidic sensors. It also does not interfere with measured signals. It is free from electromagnetic interference and poses no risk of electric shock explosion. It has been widely used in different applications includes environmental monitoring, disease diagnosis, pharmaceutical analysis, and other fields (Ali et al., 2012; Goyal et al., 2009a; Gupta et al., 2014a; Karimi-Maleh et al., 2015; Yola et al., 2014).

Optical sensors are the best mediums for transmitting signals without delay and are interference-resistant to electromagnetic radiation. In addition, they are safe and are commonly used for medical applications, particularly during MRI treatment (Taffoni et al., 2013). Recent research studies showed the potential of the optical technique for virus detection at the POC by detecting viral cell surface proteins (e.g., spike proteins). Suitable receptors such as gold, silver, and electroactive conducting polymers are used as plasmonic (Nag et al., 2020). In addition, trans-wave absorption measurement, resonance-based surface optical fiber platforms, and Surface Enhanced Raman Spectroscopy (SERS) are also potential methods for COVID-19 screening. Optical fiber sensors have different components depending on their applications. For instance, it contains various film-coated sensing nanocomposite materials such as MOS nanoparticles, piezoelectric materials, graphene oxides, and CNTs. In addition, optical sensors, including visual and photonic fiber-crystal gas sensors, detect light propagation through the device (Nazemi et al., 2019; Pawar & Kale, 2019). However, despite these advantages, optical fiber sensors have limitations in terms of miniaturization due to the size of optical fibers. Fortunately, transparent flexible materials substrate could enhance and improve its functionality.

CHAPTER 2

EXPERIMENTAL SYSTEM AND METHOD

2.1 Materials and Chemicals

The de-ionized (DI) water used in the experiments is obtained from a Milli-Q® Direct 8 Water Purification System. Acetone (≥ 99.5% ACS) and isopropyl alcohol (99% ASC) purchased from VWR Chemicals BDH® are used to clean chips. Sulfuric acid (H_2SO_4, Catalog No. A300C-212) and hydrogen peroxide (H_2O_2, Catalog No.H312-500) are all acquired from Fisher Scientific™ and used for the removal of organic contaminants. Hexamethyldisilazane (HMDS) and AZ 1512 are obtained from MicroChem Corp and used to prepare photoresist layers. AZ300 MIF developer is supplied by EDM Performance Materials Corp and used in the developing process to make the underlying pattern visible. Finally, a double-sided PSA tape (ARseal® 90880) from Adhesives Research, Inc. is adopted to use both an intermediate fluid channel and an adhesive layer to bond the top and bottom Pt μE layers. The flexible Polyethylene Terephthalate (PET) substrate is obtained from CS Hyde Company.

2.2 Fabrication of Microelectrode

The μE array's fabrication was carried out in the cleanroom of the Nanofabrication Facility in the Advanced Science Research Center, Graduate Center of the City University of New York. Figure 2 shows the general preparation process for μEs. Initially, the flexible PET substrates were thoroughly cleaned using acetone and isopropanol. Then the UV ozone cleaner (Figure 3 (a)) was employed for deep cleaning. HMDS (to promote hydrophilicity) and AZ1512 (positive photoresist) were used to prepare the photoresist layer. HMDS was spun-coated onto the substrate at 1000 rpm for 1 min (Figure 3 (b)). Subsequently, AZ1512 was spun-coated at 3000 rpm for 1

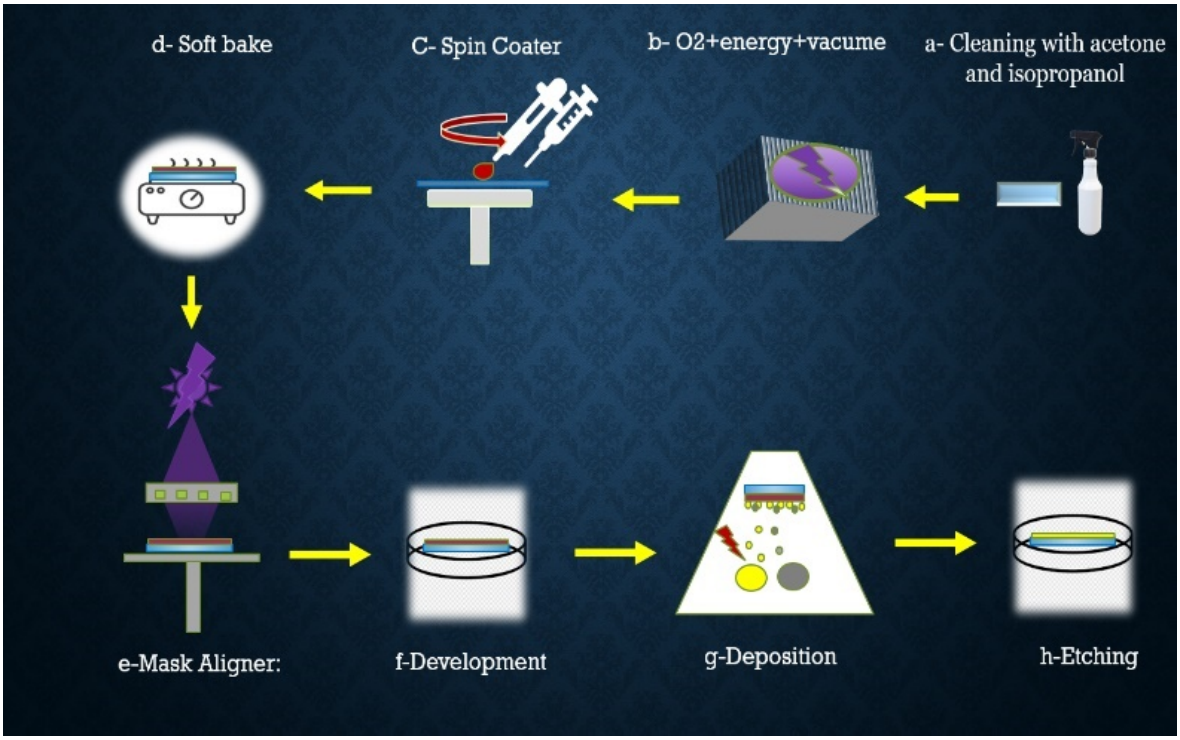

Figure 1.1. Schematic diagram of the lithography process, (a): cleaning, (b) Ozone cleaner, (c): spin Coating application, (d) soft bake, (E): Mask aligner (f): Developing (g): E-beam vapor deposition (h) lift-off process.

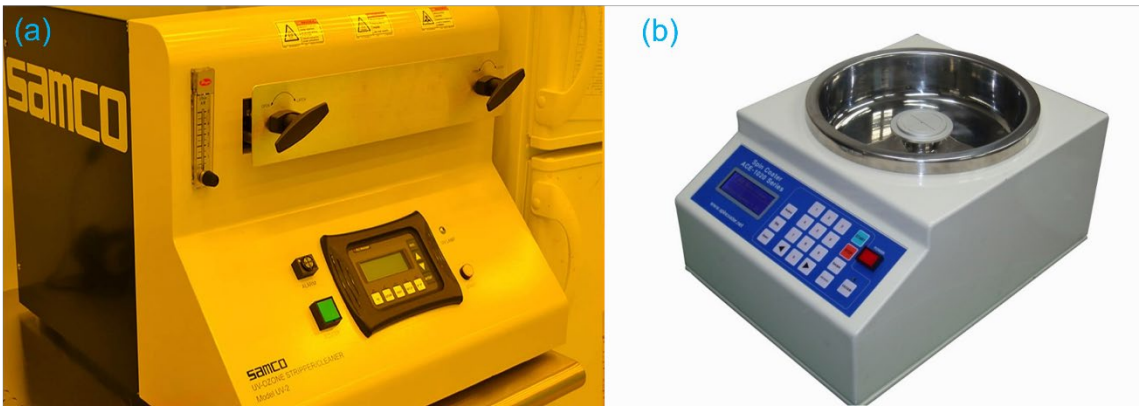

Figure 2.2. (a) SAMCO UV ozone Cleaner. (b) Picture of spinner coater.

min. After baking at 110 ^{o}C for 1 min, contact lithography was used as has been detailed elsewhere. Then the PET slides were treated with the AZ300 MIF Developer solution for ~30s to develop the electrode patterns. A Ti (10 nm)/Au (90 nm) multilayer is deposited by Electron Beam Evaporation followed by lift-off procedure. Here, each µE array has 250 fingers with each finger measuring 500 µm 10 um width x 100 µm in length x width x height, respectively.

2.3 The Photolithography Process

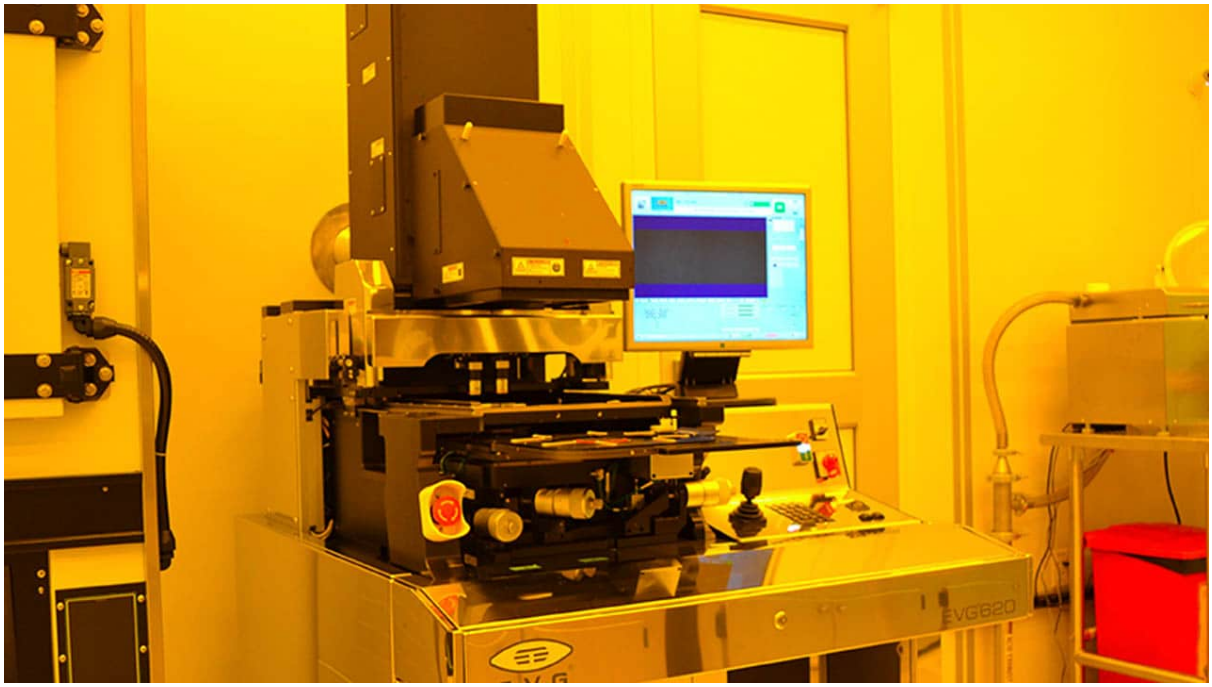

Figure 2.3. Picture of Mask Aligner.

Photolithography, or optical lithography, is a process to create micro/nanoscale microscopic patterns. Before the spin-coating of the photoresist layer, a thin layer of Hexamethyldisilane (HDMS) is applied to promote the adhesion of the photoresist material to the PET substrates. A thin film of photoresist material (AZ 1512) is created by spin-coating (Picture 4). Next, the soft-bake process at 90º–100ºC for 1 minute improved the adhesion of the photoresist material to the substrate. After that, the coating was aligned and exposed to high UV light through the photomask to make the desired µE pattern.

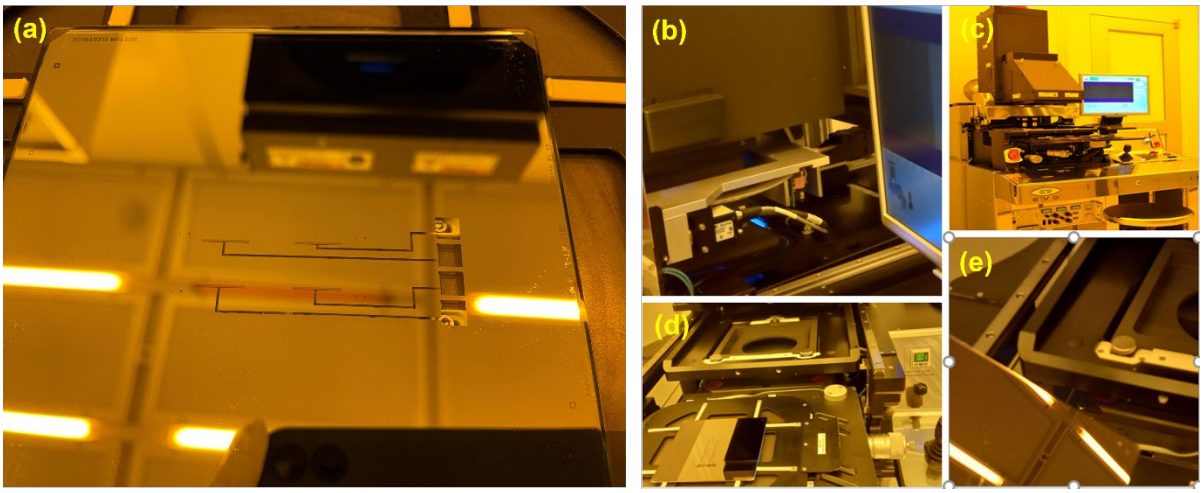

Figure 2.4. (a) Picture of chromium photomask. (b)-(e) Mask aligner with wafer chuck.

A mask aligner is a tool used to create patterns using a shadow phenomenon. Components include a UV light source, optical elements, a mask holder, substrate holder, and microscope (Figure 4, 5). Essential parameters include time, gap, type of exposure, and dosage/type of contact. Firstly, the recipe was created with the required dose. Next, the mask was loaded, the vacuum was applied, and the top and bottom alignments were performed. Next, the position and intensity were adjusted. Then, the substrate was loaded with a photomask. Finally, the substrate was exposed to UV light. Our photomask was a chromium photomask sized 5" x 5" to achieve high accuracy (up to ~1 micron) (Figure 5 (a)).

2.4 µE Inspection

The PET substrates with µE arrays were examined via an optical microscope to check the photoresist patterning and alignment quality in this step (Figure 6). We also checked the pattern height using a spectroscopic ellipsometer or stylus profiler.

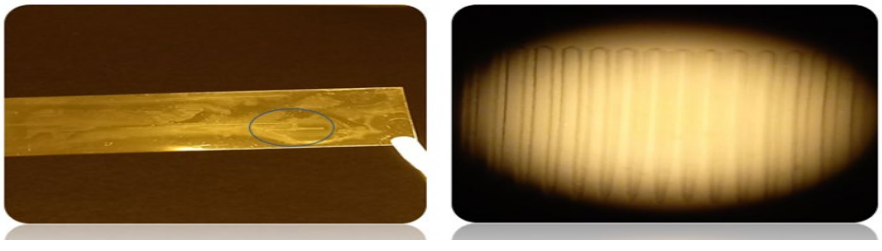

Figure 2.5. Optical image of µE array after developing process.

2.5 E-Beam Evaporator

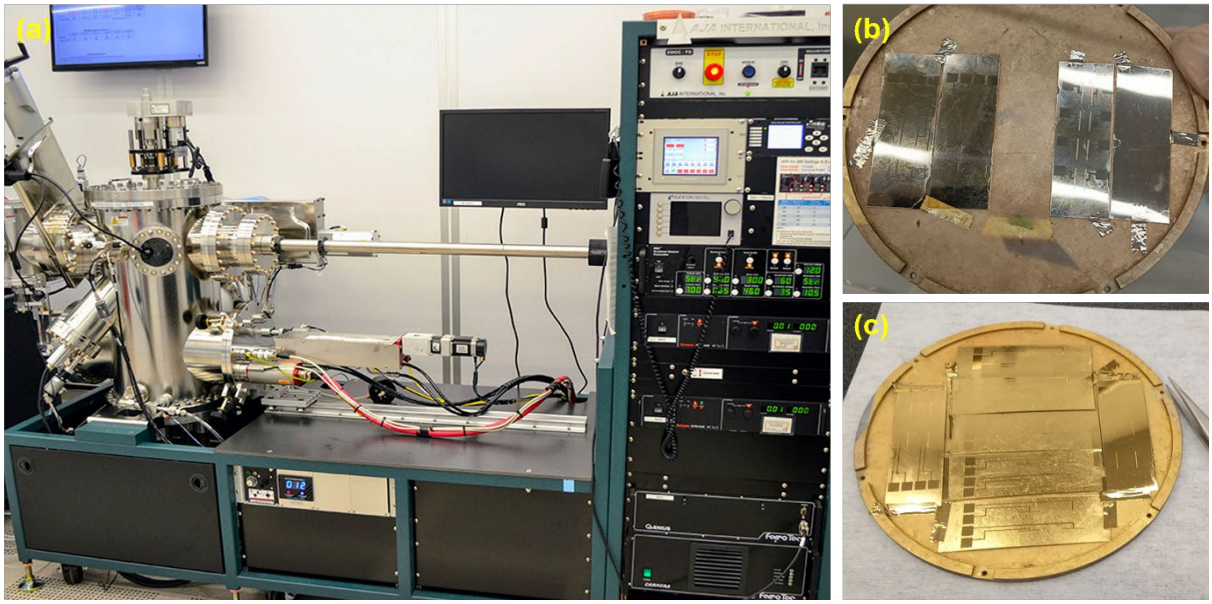

Figure 2.6. (a) E-beam evaporator (AJA international). (b) PET substrates after the Ti deposition (10 nm) (b) PET substrates after the Ti (10 nm)/Au (90 nm) multi-layer deposition.

We used an E-beam evaporator (AJA International) to deposit 10 nm of titanium (Ti) to increase the adhesion layer followed by 90 nm gold (Au) on the prepared flexible substrates (Figure 7(a)). The process of deposition in the cleanroom went through various steps. The first was loading the samples, which needed to vent to the secondary chamber to attach the pieces using Kapton tape with a proper clamp. Then, the model was transferred to the main ultra-high evacuated (UHV) chamber. The third step was recipe creation and running the deposition process. Finally, the unloading procedure comprised the same steps in reverse to get our samples to the next stage of the gold-etch or lift-off process to remove excess gold from the substrate.

2.7 Device Assembly

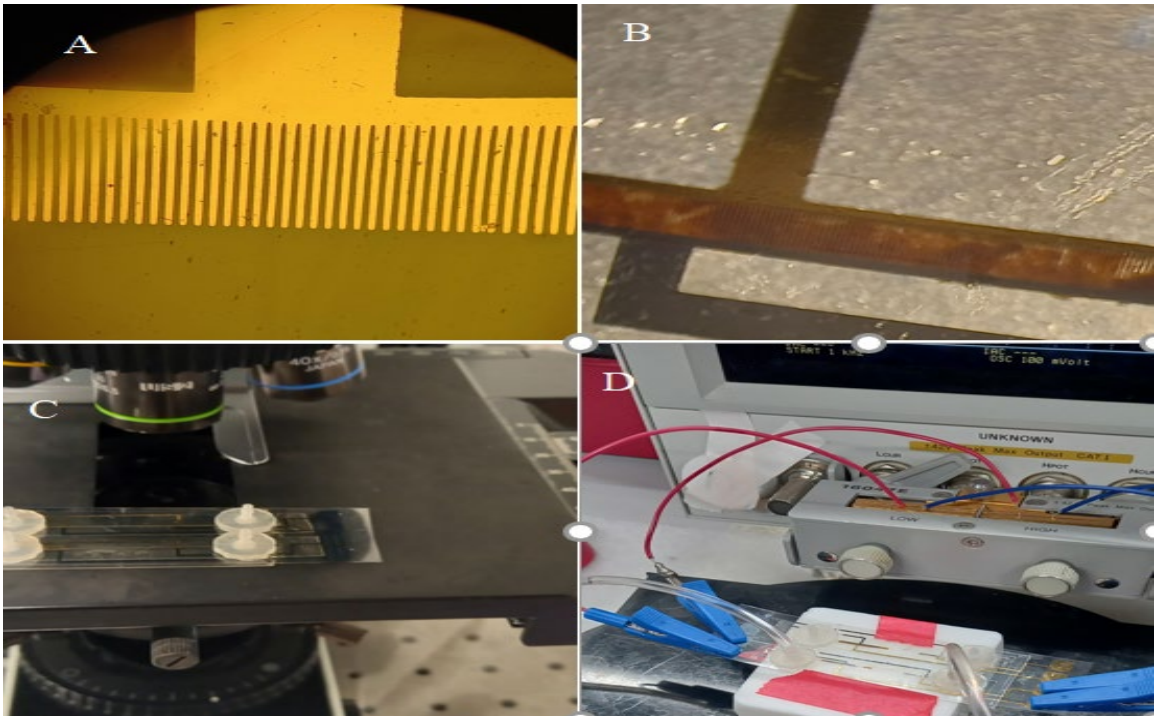

Figure 2.7. The tools used for the assembly process, (a): μE array electrodes, (b) after applying transducer material, (c) final device for measurement, (d): device is connected to the impedance analyzer EIS to get readings.

A microchannel was created using a Circuit machine in the pressure-sensitive double-sided adhesive tape. The thickness of the tape is 142 μm, including protective films on both sides. Using a microscope, they aligned the footage with a microchannel on the flexible bottom substrate with the μE array utilizing a microscope. Subsequently, transducer materials were loaded using a pipet. After that, released the protective film and applied the top flexible substrate using a microscope. Then, two holes were made from the top to the microchannel using a bench drill press (Figure 8). Next, the wires were connected to the chip using soldering tools. The KCl is diluted with DI water to get the different concentrations. The other solution was uploaded to strange, and a syringe was pumped using a controller with a flow rate of ~2 μl/min. Finally, this device is connected to the Impedance analyzer EIS to get readings.

CHAPTER 3

3.1 Result and Characterizations

3.1.1 Electrochemical Impedance Spectroscopy (EIS)

Electrochemical impedance spectroscopy (EIS) is a non-destructive electrochemical technique for measuring the impedance of a system based on the frequency of the alternating current voltage, as shown in Figure 9. EIS is a powerful nondestructive characterization tool for analyzing complex and studying system behaviors near an electrode's surface. It also provides electrochemical properties and displays highly accurate detection at low concentrations. Increased area interface between the solution and electrode allows higher sensitivity parameters, such as charge transfer resistance. The characterized system could be electrode double-layer capacitance, electrode kinetics, diffusion layer, and solvent resistance. We can also fit our experimental data to electrical circuit models using fitting programs to extract more detailed scientific information. One of the ways this is achieved is the Nyquist plot (Figure 9). Electrolyte resistance affects the electrochemical cell impedance (Rs).

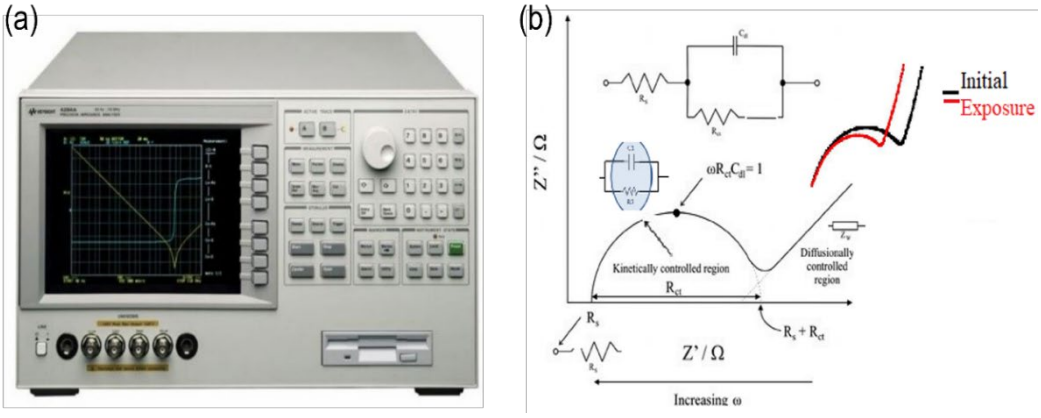

Figure 3.1. Picture of an electrochemistry impedance spectroscopy (EIS) instrument. (b) Schematic diagram of classical Randles Circuit.

The charge transfer resistance (Rct) at the interface between the electrode and the electrolyte is affected by any changes on the electrode surface (Figure 9(b)). For example, this material has a high polarization and high resistance to corrosion in corrosion measurements. The double-layer capacitance of the electrode-electrolyte interface is the electrical double layer (CDL). A binding agent such as DNA changes the charge transfer resistance because combining DNA on an electrode surface acts as a molecular wire stimulates electron transfer, increasing conductivity and reducing charge transfer resistance.

EIS experiments of the prepared chip from Chapter 2 were carried out using the following steps. Two devices were used for the experiments. The first one was empty with different concentrations of KCl. The second device was tested with two channels in service where the first channel is open and the second is packed with transducer material (Metal-Organic Frameworks). Secondly, EIS data are recorded by different electrode configurations (CE, ME, and WE). Finally, equivalent circuits under different KCl concentrations were fitted to an equivalent circuit using software such as ZsimpWin, to validate the applicability of our soft non-planar interdigitated microfluidic electrochemical cell (NP-μFEC). Our previous work has shown the potential of using the MOF Cr-MIL-101 based NP-μFEC for the detection of perfluorooctanesulfonic acid (PFOS). Considering the benefits (like more portability, less-weight) of using flexible electronics, the shift from solid/glass-based devices to soft/Polyethylene terephthalate (PET)-based devices is a future interest. Therefore, to check if the iron-based metal-organic frameworks, namely, Fe-MIL-101, can be successfully integrated into our flexible NP-μFEC and work as transducer material (that means can successfully sense the impedance changes at the solution/material surface interface and convert these changes to a measurable response).

3.2 Equivalent Circuit Analysis for Fe-MIL-101 FNP-IDμE

Four different KCl solutions are passed through the Fe-MIL-101 NP-μFEC at a flow rate of 1 μL/min. The changes in the impedance signals are collected using the EIS instrument. To analyze these signals, one possible equivalent circuit for the Fe-MIL-101 NP-μFEC is proposed and shown in Figure 9(d). Here, in the equivalent circuit, L is the parasitic inductor in the device due to external noises. Rc represents the combined resistance that comes from the external circuit, the resistance of the solution, and Fe-MIL-101 that is packed between the top and bottom μE array layers. Cc is the capacitance originating from the double-layer capacitance (Cdl) that exists in the interface between the electrolyte and Fe-MIL-101 crystals. As shown in Figure 12(b) and (c), it is assumed that the Fe-MIL-101 coverage is extensive enough that none of the ions in the electrolyte can directly interact with the top and bottom gold μE arrays. Therefore, Rct represents the charge transfer resistance associated with the electrons' transfer from the electrolyte onto the surface of Fe-MIL-101. Rct is in series with a constant phase element (Q) instead of one Warburg element (W), which is due to the inhomogeneity of the interface between the Fe-MIL-101 and electrolyte. Rct and Q are modeled parallel with the Cc because of co-occurring phenomena. Unless otherwise mentioned, all the EIS signatures (Nyquist curve) are modeled against this equivalent circuit.

3.3 Characterization of Fe-MIL-101 FNP-IDμE

The suspension solution of Fe-MIL-101 (Figure 10(a)) is loaded over the μE layer within the channel. Our previous work can provide more detailed information about the packing process (Yu et al., 2020; Li et al., 2021). Figure 10(b) shows the optical image of the packed electrode, and the corresponding cross-section SEM image is given in Figure 10(c). These images show that Fe-MIL-101 is randomly arranged but firmly packed between the top and bottom μE layers. Therefore, we can assume that the Fe-MIL-101 coverage is extensive enough that most of the ions in the electrolyte interact with Fe-MIL-101's surface instead of the top and bottom gold μEs. In addition, the introduction of the nanoporous framework of Fe-MIL-101 can bring two benefits: (i) The introduction of convection can decrease double-layer capacitance and enhance the device's signal-to-noise ratio; (ii) High accuracy by shearing off nonspecific affinity of target molecules (like PFOS, perfluorooctanoic acid (PFOA), etc.) with modified/tailored capture MOF probes.

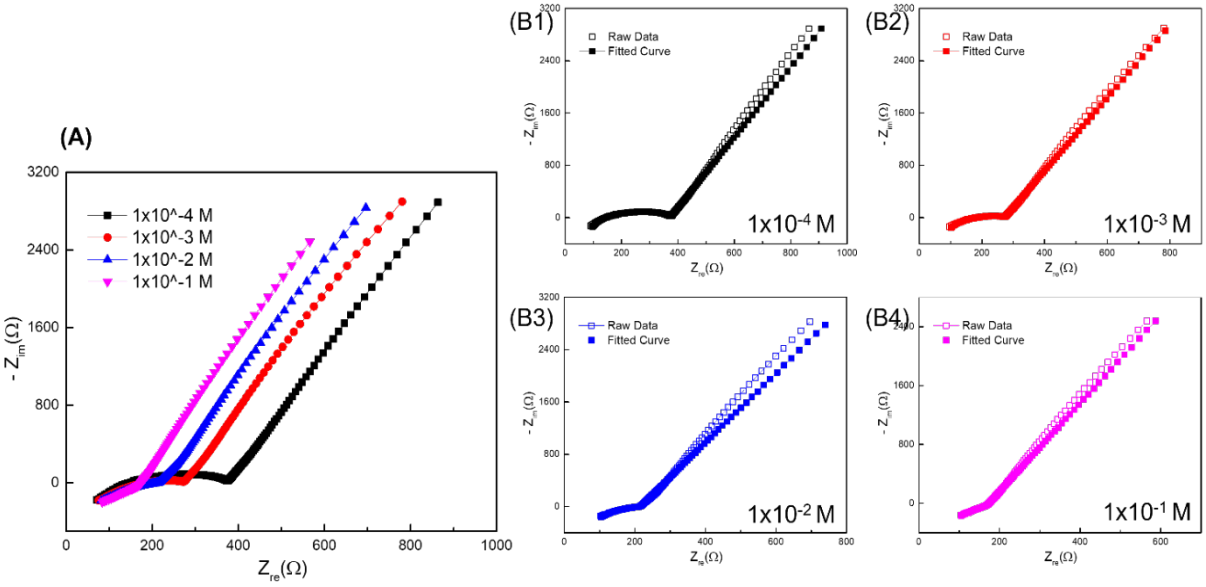

Figure 3.2. (A) Nyquist plots of Fe-MIL-101 packed NP-μFEC under different KCl concentrations. Nyquist plots of the raw data and fitted curve of Fe-MIL-101 packed NP-μFEC under different KCl concentrations of 1 x 10^{-4} M, 1 x 10^{-3} M, 1 x 10^{-2} M, 1 x 10^{-1} M

Table 3.1 Value Of Circuit Elements In The Equivalent Circuit Under Different KCl Concentrations

Device	L (Henri)	Rc (ohm)	Cc (F)	Rct (ohm)	Q (S-section)	n	Chi-square
$1x10^{-4}$ M	4.509E-7	144.4	2.103E-11	243.9	7.023E-8	0. 8829	3.02E-4
$1x10^{-3}$ M	4.729E-7	184.4	1.897E-11	102.8	6.831E-8	0. 887	2.83E-4
$1x10^{-2}$ M	4.926E-7	203.2	1.438E-11	36.98	7.41E-8	0. 8813	3.90E-4
$1x10^{-1}$ M	5.143E-7	215.1	9.337E-12	--	7.343E-8	0. 8947	2.20E-4

Figure 11 (A) shows us the EIS signatures (Nyquist plots) of Fe-MIL-101 NP-μFEC under different KCl solutions ($1x10^{-4}$ M, $1x10^{-3}$ M, $1x10^{-2}$ M, $1x10^{-1}$ M). It is observed that a gradual left-shift in the Nyquist plots appears. To figure out the changes in each element in an equivalent circuit (Figure 10(d)), the analysis work is carried out using the ZsimpWin software. The operating interface of the ZsimpWin software is shown in Figure 14. The corresponding analysis results for$1x10^{-4}$ M, $1x10^{-3}$ M, $1x10^{-2}$ M, $1x10^{-1}$ M KCl are shown in Figure 11(B1), (B2), (B3), (B4), respectively. Table 3.1 gives the detailed parameters of each component in the equivalent circuit at different concentrations. It is worthwhile to note that the low chi-squared values show that the

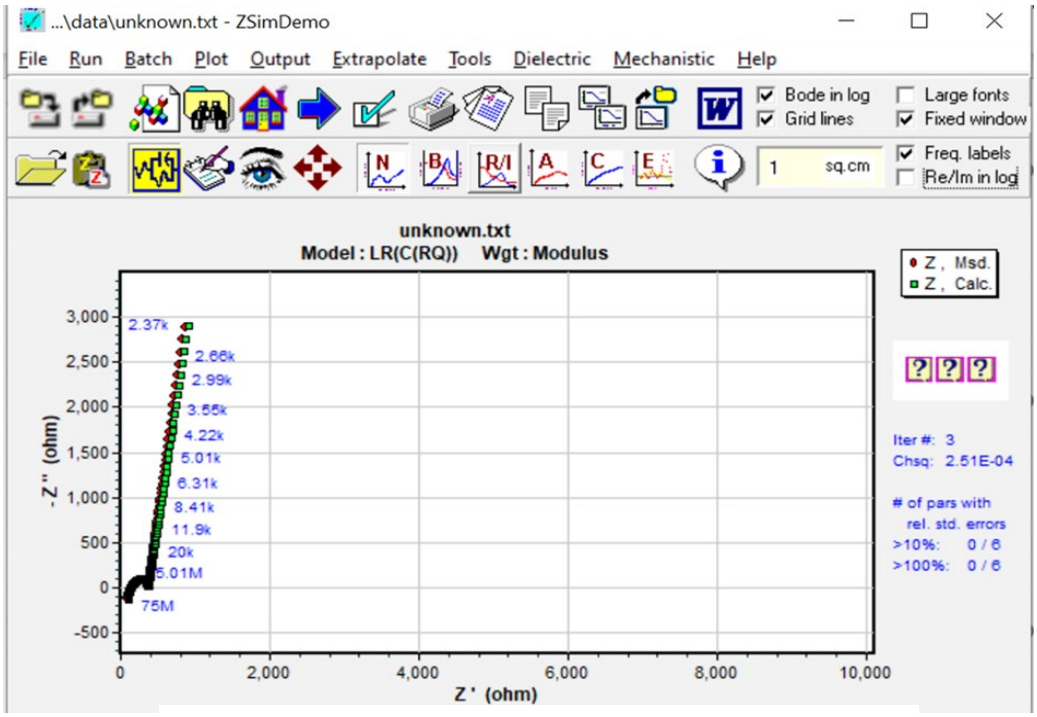

Figure 3.3. Operating interface of ZsimpWin software.

simulation results fit the experiments very well. As shown in Table 3.1, compared with other parameters, the changes in the Rct are more prominent. We observe a concomitant increase in the Rct in the EIS spectra with a decrease in concentration. Typically, Rct is measured in EIS-based sensors as a change in Rct reflects the binding of target molecules onto the electrode surface. These findings show us the potentiality of Fe-MIL-101 as transducer material in Fe-MIL-101 NP-μFEC. The use of flexible Fe-MIL-101 NP-μFEC for in-situ PFOS sensing will be one of our future works.

.

CHAPTER 4

CONCLUSION AND FUTURE WORKS

A considerable amount of study has been done on a novel design of flexible microfluidic nonplanar interdigitated microelectrodes, from material selection, manufacturing, characterizing, understanding, and analyzing to running and using the device. The device is modular, adaptable, and upgradable as needed. Also, compared to other studies, for the first time, this study covered a new packed flexible nonplanar interdigitated microelectrode sensor, different electrode configurations, WE, CE, and ME (Figure 13). The electrodes can be filled up with varying materials of the transducer. Future work may include surface enhancement to increase the adhesion of gold electrodes over the substrate. Explore materials such as PDMS and Ecoflix for the fabrication of the device. Simulation programs such as COMSOL are used to compare the results and observe the differences between simulations and experiments to enhance the design, processing steps, and performance.

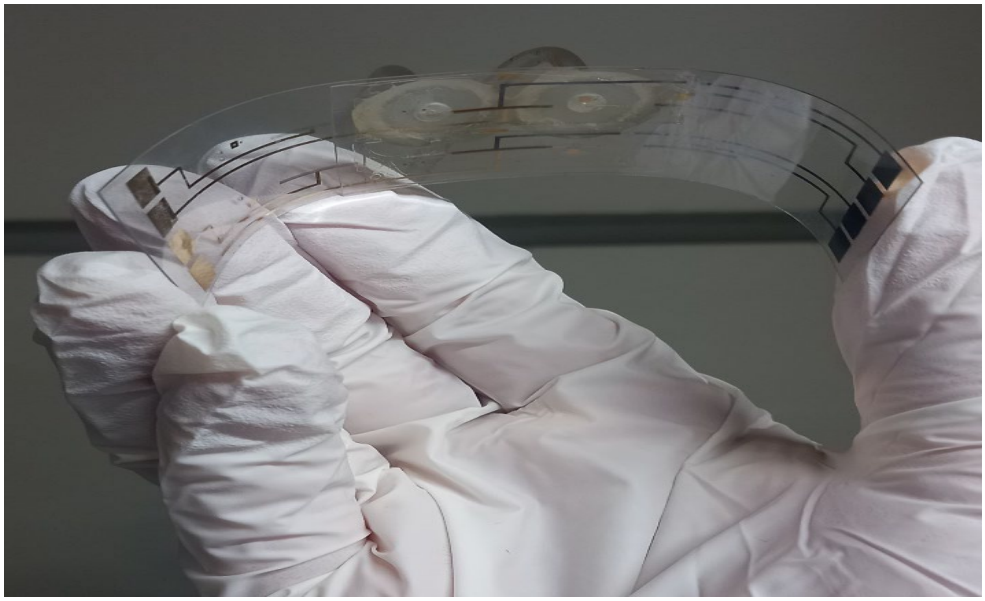

Figure 3.4. Flexible Non-Planer Interdigitated Micro Electrodes Packed with MOF (FNP-IDμE).

REFERENCES

1- Li, F., You, M., Li, S., Hu, J., Liu, C., Gong, Y., Yang, H., & Xu, F. (2020). Based point-of-care immunoassays: Recent advances and emerging trends. *Biotechnology Advances*, *39*, 107442.

2- Liu, G., Lu, M., Huang, X., Li, T., & Xu, D. (2018). Application of gold-nanoparticle colorimetric sensing to rapid food safety screening. *Sensors*, *18*(12), 4166.

3- Rong, Z., Xiao, R., Peng, Y., Zhang, A., Wei, H., Ma, Q., Wang, D., Wang, Q., Bai, Z., & Wang, F. (2021). Integrated fluorescent lateral flow assay platform for point-of-care diagnosis of infectious diseases using a multichannel test cartridge. *Sensors and Actuators B: Chemical*, *329*, 129193.

4- Shin, S. R., Zhang, Y. S., Kim, D.-J., Manbohi, A., Avci, H., Silvestri, A., Aleman, J., Hu, N., Kilic, T., & Keung, W. (2016). Aptamer-based microfluidic electrochemical biosensor for monitoring cell-secreted trace cardiac biomarkers. *Analytical Chemistry*, *88*(20), 10019–10027.

5- Uyhazi, K. E., & Bennett, J. (2021). A CRISPR view of the 2020 Nobel Prize in Chemistry. *The Journal of Clinical Investigation*, *131*(1).

6- van den Broek, J., Weber, I. C., Güntner, A. T., & Pratsinis, S. E. (2021). Highly selective gas sensing enabled by filters. *Materials Horizons*.

7- Zhu, H., Fohlerová, Z., Pekárek, J., Basova, E., & Neužil, P. (2020). Recent advances in lab-on-a-chip technologies for viral diagnosis. *Biosensors and Bioelectronics*, *153*, 112041.

8- Zhu, H., Zhang, H., Ni, S., Korabečná, M., Yobas, L., & Neuzil, P. (2020). The vision of point-of-care PCR tests for the COVID-19 pandemic and beyond. *TrAC Trends in Analytical Chemistry*, 115984.

9- Li, F., You, M., Li, S., Hu, J., Liu, C., Gong, Y., Yang, H., & Xu, F. (2020). Based point-

of-care immunoassays: Recent advances and emerging trends. *Biotechnology Advances*, *39*, 107442.

10- Liu, G., Lu, M., Huang, X., Li, T., & Xu, D. (2018). Application of gold-nanoparticle colorimetric sensing to rapid food safety screening. *Sensors*, *18*(12), 4166.

11- Rong, Z., Xiao, R., Peng, Y., Zhang, A., Wei, H., Ma, Q., Wang, D., Wang, Q., Bai, Z., & Wang, F. (2021). Integrated fluorescent lateral flow assay platform for point-of-care diagnosis of infectious diseases using a multichannel test cartridge. *Sensors and Actuators B: Chemical*, *329*, 129193.

12- Shin, S. R., Zhang, Y. S., Kim, D.-J., Manbohi, A., Avci, H., Silvestri, A., Aleman, J., Hu, N., Kilic, T., & Keung, W. (2016). Aptamer-based microfluidic electrochemical biosensor for monitoring cell-secreted trace cardiac biomarkers. *Analytical Chemistry*, *88*(20), 10019–10027.

13- van den Broek, J., Weber, I. C., Güntner, A. T., & Pratsinis, S. E. (2021). Highly selective gas sensing enabled by filters. *Materials Horizons*.

14- Zhu, H., Fohlerová, Z., Pekárek, J., Basova, E., & Neužil, P. (2020). Recent advances in lab-on-a-chip technologies for viral diagnosis. *Biosensors and Bioelectronics*, *153*, 112041.

15- Zhu, H., Zhang, H., Ni, S., Korabečná, M., Yobas, L., & Neuzil, P. (2020). The vision of point-of-care PCR tests for the COVID-19 pandemic and beyond. *TrAC Trends in Analytical Chemistry*, 115984.

16- Bakar, N. A., Rahmi, A., Umar, A. A., Salleh, M. M., & Yahaya, M. (2011). Fluorescence gas sensor using CdTe quantum dots film to detect volatile organic compounds. *Materials Science Forum*, *663*, 276–279.

17- Barroso, J., Diez-Buitrago, B., Saa, L., Möller, M., Briz, N., & Pavlov, V. (2018). Specific bioanalytical optical and photoelectrochemical assays for detection of methanol

in alcoholic beverages. *Biosensors and Bioelectronics*, *101*, 116–122.

18- Hahn, M. A., Tabb, J. S., & Krauss, T. D. (2005). Detection of single bacterial pathogens with semiconductor quantum dots. *Analytical Chemistry*, *77*(15), 4861–4869.

19- Hun, X., Wang, S., Mei, S., Qin, H., Zhang, H., & Luo, X. (2017). Photoelectrochemical dopamine sensor based on a gold electrode modified with SnSe nanosheets. *Microchimica Acta*, *184*(9), 3333–3338.

20- Jimenez, A. M. J., Moulick, A., Richtera, L., Krejcova, L., Kalina, L., Datta, R., Svobodova, M., Hynek, D., Masarik, M., & Heger, Z. (2018). Dual-color quantum dots-based simultaneous detection of HPV-HIV co-infection. *Sensors and Actuators B: Chemical*, *258*, 295–303.

21- Jin, T., Fujii, F., Sakata, H., Tamura, M., & Kinjo, M. (2005). Amphiphilic p-sulfonatocalix [4] arene-coated CdSe/ZnS quantum dots for the optical detection of the neurotransmitter acetylcholine. *Chemical Communications*, *34*, 4300–4302.

22- Lesiak, A., Drzozga, K., Cabaj, J., Bański, M., Malecha, K., & Podhorodecki, A. (2019). Optical sensors based on II-VI quantum dots. *Nanomaterials*, *9*(2), 1–24. https://doi.org/10.3390/nano9020192

23- Liu, Yongcheng, Brandon, R., Cate, M., Peng, X., Stony, R., & Johnson, M. (2007). Detection of pathogens using luminescent CdSe/ZnS dendron nanocrystals and a porous membrane immunofilter. *Analytical Chemistry*, *79*(22), 8796–8802.

24- Liu, Yueli, Wang, L., Wang, H., Xiong, M., Yang, T., & Zakharova, G. S. (2016). Highly sensitive and selective ammonia gas sensors based on PbS quantum dots/TiO2 nanotube arrays at room temperature. *Sensors and Actuators B: Chemical*, *236*, 529–536.

25- Mohammadinejad, A., Es' haghi, Z., Abnous, K., & Mohajeri, S. A. (2017). Tandem determination of mitoxantrone and ribonucleic acid using mercaptosuccinic acid-capped CdTe quantum dots. *Journal of Luminescence*, *190*, 254–260.

26- Nejdl, L., Zelnickova, J., Vaneckova, T., Hynek, D., Adam, V., & Vaculovicova, M. (2018). Rapid preparation of self-assembled CdTe quantum dots used for sensing of DNA in urine. *New Journal of Chemistry*, *42*(8), 6005–6012.

27- Pawar, D., & Kale, S. N. (2019). A review on nanomaterial-modified optical fiber sensors for gases, vapors and ions. *Microchimica Acta*, *186*(4). https://doi.org/10.1007/s00604-019-3351-7

28- Seekaew, Y., Lokavee, S., Phokharatkul, D., Wisitsoraat, A., Kerdcharoen, T., & Wongchoosuk, C. (2014). Low-cost and flexible printed graphene–PEDOT: PSS gas sensor for ammonia detection. *Organic Electronics*, *15*(11), 2971–2981.

29- Sotelo-Gonzalez, E., Fernandez-Argüelles, M. T., Costa-Fernandez, J. M., & Sanz-Medel, A. (2012). Mn-doped ZnS quantum dots for the determination of acetone by phosphorescence attenuation. *Analytica Chimica Acta*, *712*, 120–126.

30- Su, S., Fan, J., Xue, B., Yuwen, L., Liu, X., Pan, D., Fan, C., & Wang, L. (2014). DNA-conjugated quantum dot nanoprobe for high-sensitivity fluorescent detection of DNA and micro-RNA. *ACS Applied Materials & Interfaces*, *6*(2), 1152–1157.

31- Tai, H., Duan, Z., Wang, Y., Wang, S., & Jiang, Y. (2020). based sensors for gas, humidity, and strain detections: A review. *ACS Applied Materials & Interfaces*, *12*(28), 31037–31053.

32- Wang, B., Chen, M., Zhang, H., Wen, W., Zhang, X., & Wang, S. (2017). A simple and sensitive fluorometric dopamine assay based on silica-coated CdTe quantum dots. *Microchimica Acta*, *184*(9), 3189–3196.

33- Wei, F., Wu, Y., Xu, G., Gao, Y., Yang, J., Liu, L., Zhou, P., & Hu, Q. (2014). Molecularly imprinted polymer based on CdTe@ SiO 2 quantum dots as a fluorescent sensor for the recognition of norepinephrine. *Analyst*, *139*(22), 5785–5792.

34- Wu, F., Zhou, B., Wang, J., Zhong, M., Das, A., Watkinson, M., Hing, K., Zhang, D.

W., & Krause, S. (2019). Photoelectrochemical Imaging System for the Mapping of Cell Surface Charges. *Analytical Chemistry*, *91*(9), 5896–5903. https://doi.org/10.1021/acs.analchem.9b00304

35- Wu, P., Huang, R., Li, G., He, Y., Chen, C., Xiao, W., & Ding, P. (2018). Optimization of synthesis and modification of ZnSe/ZnS quantum dots for fluorescence detection of Escherichia coil. *Journal of Nanoscience and Nanotechnology*, *18*(5), 3654–3659.

36- Xue, L., Zheng, L., Zhang, H., Jin, X., & Lin, J. (2018). An ultrasensitive fluorescent biosensor using high gradient magnetic separation and quantum dots for fast detection of foodborne pathogenic bacteria. *Sensors and Actuators B: Chemical*, *265*, 318–325.

37- Zhao, D. A. I., Zhang, J., Quanxi, D., Ning, G. U. O., Shichao, X. U., Bo, S. U. N., & Yuehua, B. U. (2007). Adaption of Au nanoparticles and CdTe quantum dots in DNA detection. *Chinese Journal of Chemical Engineering*, *15*(6), 791–794.

38- Zhao, Y., Hu, X. guang, Hu, S., & Peng, Y. (2020). Applications of the fiber-optic biochemical sensor in microfluidic chips: A review. *Biosensors and Bioelectronics*, *166*(July), 112447. https://doi.org/10.1016/j.bios.2020.112447

39- Emergent research (2020) Biosensors Market to Reach USD 33.85 Billion By 2027 | CAGR of 7.3%: Emergen Research retrieved from: https://www.emergenresearch.com/industry-report/biosensors-market

40- Cheng, Y. H., Moura, P. A. R., Zhenglong, L., Feng, L., Arokiam, S., Yang, J., ... & Basuray, S. (2019). Effect of electrode configuration on the sensitivity of nucleic acid detection in a nonplanar, flow-through, porous interdigitated electrode. *Biomicrofluidics*, *13*(6), 064118.

41- Arshavsky-Graham, S., & Segal, E. (2020). Lab-on-a-Chip Devices for Point-of-Care Medical Diagnostics.

42- Chen, X., Liu, C., & Mao, S. (2020). Environmental analysis with 2D transition-metal

dichalcogenide-based field-effect transistors. Nano-Micro Letters, 12(1), 1–24.

43- Jaywant, S. A., & Arif, K. M. (2019). A comprehensive review of microfluidic water quality monitoring sensors. Sensors, 19(21), 4781.

44- Jenkins, C., & Orsburn, B. (2020). In silico approach to accelerate the development of mass spectrometry-based proteomics methods for detection of viral proteins: Application to COVID-19. BioRxiv.

45- Katalani, C., Booneh, H. A., Hajizade, A., Sijercic, A., & Ahmadian, G. (2020). CRISPR-Based Diagnosis of Infectious and Noninfectious Diseases. Biological Procedures Online, 22(1), 1–14.

46- Molaei, M. J. (2019). A review on nanostructured carbon quantum dots and their applications in biotechnology, sensors, and chemiluminescence. Talanta, 196, 456–478.

47- Ocampo, C. S., Lopez Badilla, G., Romero Samaniego, E., Toledo Perea, S. L., & Campos Garcia, J. (2015). SEM and AES analysis of corrosion in steel cans of meat and poultry food industry influenced by microorganisms affecting the competitiveness in northwest of Mexico. Journal of Spectroscopy, 2015.

48- Parkhey, P., & Mohan, S. V. (2019). Biosensing applications of microbial fuel cell: Approach toward miniaturization. In Microbial Electrochemical Technology (pp. 977–997). Elsevier.

49- Popoola, O. A. M., Stewart, G. B., Mead, M. I., & Jones, R. L. (2016). Development of a baseline-temperature correction methodology for electrochemical sensors and its implications for long-term stability. Atmospheric Environment, 147, 330–343.

50- Randviir, E. P., & Banks, C. E. (2013). Electrochemical impedance spectroscopy: an overview of bioanalytical applications. Analytical Methods, 5(5), 1098-1115.

51- Zhang, C., & Du, X. (2020). Electrochemical sensors based on carbon nanomaterial used in diagnosing metabolic disease. Frontiers in Chemistry, 8.